Curvelet Based Image De-noising using *beta-trim* Shrinkage for Magnetic Resonance Images

A. Sumaiya Begum[1] and S. Poornachandra[2]

[1]Department of ECE, RMD Engineering College, Chennai, India.
[2]Department of ECE, SNS College of Engineering, Coimbatore, India.

DOI: http://dx.doi.org/10.13005/bbra/1715

(Received: 20 December 2014; accepted: 23 January 2015)

Curvelet transform for de-noising Magnetic Resonance images corrupted with Rician noise using a newly proposed technique called *beta-trim* shrinkage. In this paper *beta-trim* shrinkage is combined with Bayesian thresholding technique to recover the image corrupted with noise. The classical wavelet transform codes homogenous regions effectively. However for improved image perception edges need to be preserved. Curvelet transform is well suited for edge preservation. Curvelet transform offers a sharp detection of linear and curvilinear features thus providing visually high-resolution images. Experiments were performed on several images. Results show that a significant level of noise is reduced by the proposed *beta-trim* method using Bayes thresholding rule when compared to classical methods. An appreciably high value of Peak Signal to Noise Ratio (PSNR), Structural Similarity Index (SSIM), Correlation Coefficient (CC) and fairly lesser value of MSE (Mean square error) are obtained by the proposed method.

Key words: Curvelet Transform, Wavelet Transform, USFFT, Wrapping, Shrinkage.

The purpose of image de-noising is to reduce the noise level in the image and to restore the original image. Most of the images are corrupted by additive White Gaussian noise.

A shrinkage method compares empirical wavelet coefficient with a threshold and is set to zero if its magnitude is less than the threshold value[3]. The threshold acts as an oracle, which distinguishes between the significant and insignificant coefficients. Shrinkage of empirical wavelet coefficients works best when the underling set of the true coefficients of *f* is sparse. In wavelet shrinkage, energy of the function will be concentrated in a few coefficients[3-6]. Therefore, nonlinear function in wavelet domain will retain few larger coefficients representing the function while the coefficients below threshold will be reduced to zero. The development of practical algorithms requires that one choose the appropriate shrinkage rule and an equally appropriate threshold of wavelet coefficients empirically. The choice of shrinkage rule plays a vital role in image de-noising. The most frequently used shrinkage methods are hard and *soft*.

* To whom all correspondence should be addressed.
E-mail: sumizahoor@gmail.com

Wavelet Transform

Extensive research has been carried out on image de-noising using wavelet transform. Initially linear methods using Weiner filter [22], were deployed. These methods though simple had the disadvantage of over smoothening. Donoho and others put forward *soft* and *hard* wavelet de-noising methods [11-12]. In the above mentioned methods the image data is transformed into wavelet space in the form of wavelet coefficients. The coefficients at the coarsest scale are left intact, while the coefficients at all the other scales are threshold via different thresholding techniques. Other methods

based on partial differential equations and Independent Component analysis has also gained much significance [4].

Wavelet Transform decomposes the signal into a number of sub bands with approximate (low frequency) and detail coefficients (high frequency). An appropriate thresholding rule is applied to coefficients in the detail sub-bands. The de-noised image is then obtained by applying inverse wavelet transform. Discrete Wavelet Transform has made a high impact in the field of signal processing, image processing and several other applications.

The main drawback of wavelet is that it lacks sparse representation along C^2 curve. However the usage of wavelet transform has reduced to a great extent due to poor directionality. Complex wavelets were introduced to overcome this disadvantage. The complicated design process involved, coupled with poor reconstruction properties and filter design has undermined its usage [20,35]. The Dual tree complex wavelet Transform is characterized by features such as directional selectivity (six directions) much better when compared to DWT (3 directions), approximate shift invariance, limited redundancy and efficient O(N) computation [25-26]. Though there was an improvement in directional selectivity still it is limited. Wavelets were not the best for sparse representation of natural images. Hence Multi scale Geometric analysis was proposed and developed. Several multiscale directional transforms have been proposed. These transforms are characterized by anisotropy and high directionality. These transforms include Ridgelets [17,21], Curvelets [8,14], Contourlets [24], Directionlets [33], Steerable Wavelets [16, 34], Gabor Wavelets [32], Wedgelets [7], Surfacelets [37], Bandlets [15, 30], Platelets [27] and Shearlets [10, 23].

Steerable wavelets are translational invariant and rotation invariant with respect to the position and orientation of the image. It provides a linear, multi-scale, multi-orientation image decomposition. The directional derivative operators, which form the basis functions of steerable pyramid, can be altered in size and orientations. The most important advantage of steerable wavelets is the polar-separable decomposition in the frequency domain, which allows independent representation of scale and orientation. However it has the disadvantage of complex filter design and the representation being overcomplete by a factor of 4k/3, where k represents the number of orientations.

Gabor wavelets are obtained from Gabor kernel function by Time-Frequency shifts. Gabor function is a product of elliptical Gaussian and a complex plane wave. They play a major role in many computer vision applications, modeling biological vision and texture analysis. Applications of Gabor wavelets suggested that the precision in resolution achieved through redundancy may be a more relevant issue in brain modeling, and that orientation plays a key role in the primary visual cortex. However, 1D or 2D Gabor wavelets do not form orthonormal bases. They are called non-orthogonal wavelets.

Do and Vetterli constructed Contourlet by combining Directional filter bank with Laplacian pyramid [24]. The directional filter bank has high directional selectivity and provides effective directional decomposition of 2-D signals, which makes it popular in image processing applications. Contourlet transform is an efficient multiscale geometric analysis tool, which aims at better image representation of 2-D images. Contourlet transform provides near optimal representation of images as it allows for flexible number of directions at each scale. The main difference between Contourlet and Curvelet transform is that Contourlet transform is based on discrete rectangular grids. However when compared to Curvelet the Contourlet functions lead to more oscillations along sharp edges leading to artifacts in denoising and compression.

Surfacelets are higher dimensional extensions of Contourlets. In case of Surfacelet, N-directional filter banks (NDFB) are combined with multiscale pyramid. This is similar to Contourlet transform in which 2-D DFB is combined a multiscale decomposition. Surfacelets efficiently extracts and represents surface-like singularities in multidimensional data. Surfacelets are used in a wide range of applications such as computer vision analysis biomedical image processing and video processing [37].

Wedgelets are functions with a variety of locations, scales and orientation. Wedgelets find application in optimal represention of objects in the horizon model.

Bandlets are obtained by applying local orthogonal transformation to wavelet coefficients. The bandlet transform exploits the anisotropic regularity (which appears along edges in images) by constructing orthogonal vectors that are elongated in the direction where the function has a maximum of regularity [15, 30]. Similar to other directional transforms platelets are capable of representing edges at various scales, locations and orientations. Platelet representations are well suited for Poisson data. Due to speedy computation they find applications in variety of fields such as confocal microscopy, infrared Imaging, image restoration, and emission tomography [27].

Unlike Curvelets, In case of Shearlets the mother Shearlet function is characterized by parameters such as scale, translation and shear parameter. Of these, the shear parameter captures directional features like orientations of curves in images while providing sparse decompositions. Both the transforms are found to be similar in discrete implementation and decay rates [10,23].

Directionlet transform is used to capture anisotropic geometric structures in multiple directions from a low-resolution image. Integer lattices are applied to scaling and filtering operations. Since all the basic operations are one dimensional (1-D) the transform retains the separability and simplicity of standard two dimensional (2-D) wavelet transform. Furthermore, it provides an efficient tool for nonlinear approximation of images. Recently Curvelet transform has emerged as a widely used tool for image de-noising.

Ridgelet transform

In order to handle higher dimensional singularities in 1999, Candes and Donoho proposed Ridgelet transform. Ridgelet transform is an anisotropic geometric transform capable of optimally representing straight-line singularities. These first generation Curvelets [13] include sub-band decomposition followed by Ridgelet analysis [17, 21] of the radon transform of an image. Wavelet transforms are good at point singularities, for line singularities, Ridgelet transform was introduced. The line singularity on applying radon transform becomes point singularity. Wavelet transform can then be used handle this point singularity. This is the main idea behind Ridgelets.

Let $\psi_{a,b,\theta}$ represent a bivariate ridgelet in R^2 with the parameters indexed by 'a' > 0 a scaling parameter, 'θ' an orientation parameter and 'b' a location scalar parameter. The ridgelet function is then given by

$$\psi_{a,b,\theta} = a^{-1/2}\psi((x\cos\theta + y\sin\theta - b)/a) \quad ...(1)$$

This function is constant along the lines. Wavelet is transverse to these ridges. Given an integrable bivariate function , then its ridgelet coefficients are given by

$$R(a,b,\theta) = \int \psi_{a,b,\theta} f(x,y)\,dx\,dy \quad ...(2)$$

Radon Transform

Radon transform in two dimensions, is the integral transform consisting of the integral of a function over straight lines. The Radon transform finds applications in computed axial tomography, electron microscopy, reflection seismology and in the solution of hyperbolic partial differential equations [6,18-19].

The radon Transform for a function is given by

$$R(\theta,t) = \int f(x_1,x_2)\delta(x_1\cos\theta + x_2\sin\theta - t)dx_1dx_2$$

$f(x,y)$ ...(3)

The main disadvantage of Ridgelets is that they can very well represent objects with straight line singularities but they lack in representing local line and curved singularities.

Curvelet transform

In order to overcome these disadvantages second generation Curvelets were introduced. The second generation Curvelets is simpler and transparent. This new architecture excludes the use of Ridgelet transform. Curvelet transform can implemented using two distinct digital implementations namely, Unequally-Spaced Fast Fourier Transform (USFFT) and the Wrapping-based Transform. Both the versions are fast, invertible and less redundant [8,14]. However the two variants differ by the choice of the spatial grid used to translate Curvelets at each scale and angle. USFFT uses a decimated rectangular grid tilted along the main direction of each Curvelet. In case of USFFT Curvelet coefficients are obtained by irregularly sampling the Fourier coefficients of an image. The second method includes wrapping the spatially selected Fourier samples. Even though

similar results are obtained using both the methods, the latter version is used throughout this paper due to simplicity in implementation.

Continuous Time Curvelet Transforms

Consider a spatial variable 'x', a frequency domain variable 'ù' and polar coordinates 'r' and 'è' in the frequency domain. Let and represent radial and angular windows respectively. W takes positive real arguments with r " (1/2, 2) and V takes real arguments with t " [-1, 1].

These windows obey the admissibility condition

$$\sum_{j=-\infty}^{\infty} W^2(2^j r)=1, \quad r \in (3/4, 3/2);$$
$$\sum_{l=-\infty}^{\infty} V^2(t-l)=1, \quad t \in (-1/2, 1/2). \qquad ...(4)$$

Now, for each j e" , the frequency window given by in the Fourier domain is given by

$$U_j(r,\theta)=2^{-3j/4} W(2^{-j} r) V\left(\frac{2\lfloor j/2 \rfloor \theta}{2\Pi}\right) \qquad ...(5)$$

Where represents the integer part of j/2.

Digital Curvelet transform via Wrapping

The above digital implementation is based on the choice of spatial grid used to translate Curvelets at each scale and angle. Instead of a tilted grid a regular rectangular grid is used to translate Curvelets. The spatial grid used to translate Curvelets in this case is same for every angle within each quadrant, yet each Curvelet undergoes proper orientation. Hence this version of the transform is much simpler to implement.

The algorithm for the implementation of FDCT via wrapping is as follows:

1. Consider a two dimensional function , $0 \le t_1, t_2 \le \omega$, in the Descartes coordinate. The Fourier samples $\hat{f}[n_1, n_2], -n/2 \le n_1, n_2 < n/2$ are obtained on applying 2D FFT.
2. The Fourier samples $\hat{f}$ for each scaleand j angle are multiplied by the window function $\hat{U}_{j,l}$, to obtain the product $\tilde{U}_{j,l}[n_1, n_2]\hat{f}[n_1, n_2]$.
3. The product is then wrapped around the origin to obtain $\tilde{f}_{j,l}[n_1, n_2]=W(\tilde{U}_{j,l}\hat{f})[n_1, n_2]$,

Where the range for and is now and for in the range from

4. Apply 2D IFFT to each $\tilde{f}_{j,l}$ and obtain the discrete coefficients $c^D(j,l,k)$.

The above procedure is as fast as $O(n^2 \log n)$. In the wrapping approach both forward and inverse operations are performed in $O(n^2 \log n)$ operations.

Objective

Almost every image is corrupted by noise. De-noising plays a vital role in many of the current research areas. Image De-noising aims to recover an original image from a noisy observation corrupted by an additive white Gaussian noise (AWGN). Assume $y_{i,j}$ to be the original $K \times K$ image

where corrupted by AWGN $n_{i,j}$

$$x_{i,j} = y_{i,j} + n_{i,j} \qquad ...(6)$$

The goal of de-noising is to estimate of by reducing . The MR Images are however corrupted by Rician noise, which is Multiplicative in nature

Noise in MRI – Rician noise

Magnetic resonance images are invariably corrupted by random noise during transmission and acquisition process. Noise in MRI trammels clinical and diagnostic analysis. Image intensity in magnitude MR image follows Rician distribution. MRI uses magnitude images as they are devoid of the artifacts due to phase information. MR magnitude images are obtained by calculating the magnitude for each and every pixel, from real and imaginary images. This mapping is however, non-linear and therefore does not follow Gaussian distribution. Hence the bias due to Rician distribution needs to be corrected.

MR Images comprise of real and imaginary components with similar variance and Gaussian noise distribution. The magnitude MR images computed from the real and imaginary parts follow Rician distribution. The Rician noise built from Gaussian is given by:

$$x_r(i) = y(i) + n_1(i), n_1(i) \sim N(0,\sigma),$$
$$x_i(i) = n_2(i), n_2(i) \sim N(0,\sigma), \qquad ...(7)$$

where, represents the original image. represents the imaginary component and represents the real component.represents the

standard deviation of the Gaussian noise. Then the noisy image is computed as follows

$$x(i) = \sqrt{x_r(i)^2 + x_i(i)^2} \quad ...(8)$$

The bayesian threshold

Threshold selection plays a major role in de-noising technique as, a very low value of threshold will lead to noise retention and a high value of threshold will results in smoothening effect. Several methods of selecting threshold have introduced and investigated [28-29]. Bayesian approach is an important thresholding technique, which has been attracting attention due to its adaptive nature. Bayesian approach provides the means to incorporate prior knowledge in data analysis. Bayesian approach is based on posterior probability. Bayes law states that the posterior probability is proportional to the product of the likelihood and the prior probability. In this approach the threshold value depends on noise variance and standard deviation of the signal. The Bayes method is effective for images contaminated by Gaussian noise. In this approach noise variance is estimated by a robust median estimator [5,31]. In case of wavelet transform the robust median estimator is expressed as

$$\hat{\sigma} = \frac{Median(|p_{i,j}|)}{0.6745} \quad p_{i,j} \in subband \quad ...(9)$$

In case of wavelet transform the orientations are limited to three. However Curvelet transform has more orientations with tight frame. Curvelet coefficients are expressed in the form of cells. Hence in case of Curvelet transform the robust median estimator is expressed as follows

$$\hat{\sigma} = \frac{Median(|p\{i\}\{j\}|)}{0.6745} \quad |p\{i\}\{j\}| \in subband \quad ...(10)$$

Signal variance is estimated as $\hat{\sigma}_x^2 = \max(\hat{\sigma}_u^2 - \hat{\sigma}^2, 0)$

Where $\hat{\sigma}_u^2$ is the estimate of variance of observations.

Bayes threshold can be obtained as follows

$$\lambda = \frac{\hat{\sigma}^2}{\hat{\sigma}_x^2} \quad ...(11)$$

The *soft* shrinkage technique with Bayes threshold is given as

$$\delta_\lambda^{soft}(x_{i,j}) = \text{sgn}(x_{i,j}) * \max(x_{i,j} - \lambda, 0)$$

While the *hard* shrinkage technique with Bayes threshold is given as

$$\delta_\lambda^{hard} = x_{i,j} \quad for\ x_{i,j} > \lambda$$
$$= 0 \quad otherwise \quad ...(13)$$

Of the two methods, *soft* shrinkage technique is more effective when compared to *hard* shrinkage technique. The *hard* shrinkage technique is not continuous at the threshold resulting in oscillations in the recovered signal. *soft* shrinkage technique also has some disadvantages. In case *soft* shrinkage technique there are deviations between image coefficients and threshold coefficients, which in turn results in the lack of accuracy in the recovered signal.

In 2009 a new shrinkage technique called extrim shrinkage was introduced [1-2].

The ex-trim shrinkage model is expressed as:

$$\delta^{extrim}(x_{i,j}) = \text{sgn}(x)(\exp^{|x|^n} - 1) \quad ...(14)$$

The factor 'n' represents the scaling parameter, which scales the shrinkage function to the image dimensions.

The *ex-trim* shrinkage technique was formulated with the perspective of improving the denoising technique without threshold requirement. The *ex-trim* shrinkage includes non-linearity and thus excludes the disadvantages of linear methods such as *soft* and *hard* shrinkage functions. The point wise distribution of *ex-trim* shrinkage is comparable with *soft* hence it retains the same function stability of soft shrinkage model. However *extrim* shrinkage is not included in the experimental analysis due to the absence of threshold and incompatibility of extrim shrinkage in Curvelet domain. Hence in this paper a new shrinkage technique is proposed.

beta-trim Shrinkage

The newly proposed technique namely, *beta-trim* shrinkage is based on a set of exponential functions given in equation (15). In case of *beta-trim* shrinkage, the insignificant empirical coefficients are shrunk in a non-linear manner using the following equation.

$$\delta_\lambda^{\beta-trim}(x_{i,j}) = \left(\frac{1-\exp(-x)}{1+\exp(-x)}\right) * \lambda + \left(\frac{1-\exp(-x)}{1+\exp(-x)}\right) \quad ...(15)$$

Where represents the Bayesian threshold. The above equation shows that it involves exponential function similar to extrim shrinkage. However it involves a Bayesian threshold. The point wise distribution functions of *soft*, *hard*, *extrim* and *beta-trim* are shown in figure 1. From the figure it is found that though *beta-trim* function includes an exponential function similar to extrim shrinkage, its distribution function resembles *soft* shrinkage function.

However the slope of *beta-trim* is different when compared to *soft* shrinkage technique. In *soft* and *hard* thresholding linear filtering is used to de-noise the image. Linear de-noising methods are not so effective when transient non-stationary wide-band components are involved since they have similar spectrum as that of the noise. Most of the shrinkage methods rely on the basic idea that the energy of a signal (with some smoothness) will often be concentrated in a few coefficients while the energy of noise is spread among all coefficients. Therefore, the nonlinear shrinkage function will tend to keep a few larger coefficients representing the signal while the noise coefficients will tend to reduce to zero. Thus in the proposed technique nonlinearity is introduced. Another important advantage of *beta-trim* shrinkage is the smooth transition of the curve in the region, which tries to shrink the insignificant coefficients towards zero. The distribution characteristic of *beta-trim* shrinkage is an adaptive one. As the noise tends to increase, larger number of redundant empirical coefficients is shrunk to zero on the contrary lesser number of coefficients is shrunk, as noise tends to reduce. The de-noising procedure is explained in figure 2.

The major advantage of *beta-trim* shrinkage is its near optimal restoration of image, high noise rejection capability and its functional stability. *beta-trim* shrinkage works as function of exponential functions, with a pointwise distribution function similar to that of *soft* shrinkage.

Experiments and parametric analysis

The test includes three different images, corrupted by Gaussian noise. In this test the following methods were implemented for de-noising.

- *soft* shrinkage using bayesian threshold
- *hard* shrinkage using bayesian threshold
- Proposed shrinkage using bayesian threshold

In this section we use Curvelet based de-noising using *beta-trim* shrinkage in order to recover the image. We consider three 8-bit gray scale Brain MR images for the experiment. The noisy images were tested with the above-mentioned de-noising techniques and the quality of the recovered image was estimated. The quality of the image was determined using the following parameters namely Peak Signal to Noise Ratio (PSNR) , Mean Square Error (MSE) Structural Similarity Index (SSIM) and Correlation Coefficient (CC). The quality metrics thus obtained are listed in Tables 1-6.

The PSNR is given by

$$PSNR = 20\log\frac{255^2}{\frac{1}{MN}\sum_{i=1}^{M}\sum_{j=1}^{N}(y(i,j)-\hat{y}(i,j))^2} \quad ...(16)$$

The MSE is given by

$$MSE = \frac{1}{MN}\sum_{i=1}^{M}\sum_{j=}^{N}(y(i,j)-\hat{y}(i,j))^2 \quad ... (17)$$

Structural Similarity Index (SSIM) gives the structural similarity between two images

$$SSIM = \frac{(2\bar{y}\bar{\hat{y}}+C_1)(2\sigma_{y\hat{y}}+C_2)}{((\bar{y})^2+(\bar{\hat{y}})^2+C_1)(\sigma_y^2+\sigma_{\hat{y}}^2+C_2)} \quad ...(18)$$

The Correlation coefficient (CC) is given by

$$CC = \frac{\sum_{i=1}^{M}\sum_{j=1}^{N}(y_{i,j}-\bar{y}_{i,j})(\hat{y}_{i,j}-\bar{\hat{y}}_{i,j})}{\sqrt{\sum_{i=1}^{M}\sum_{j=1}^{N}(y_{i,j}-\bar{y}_{i,j})^2\sum_{i=1}^{M}\sum_{j=1}^{N}(\hat{y}_{i,j}-\bar{\hat{y}}_{i,j})^2}} \quad ...(19)$$

Where

M - width of the image

N - height of the image

$y(i, j)$ - Original image

$\hat{y}(i, j)$ - de-noised image

σ_y - Standard Deviation of the original image

$\sigma_{\hat{y}}$ - Standard Deviation of the De-noised image

$\sigma_{y\hat{y}}$ - Covariance of y and

$C_1 = (k_1 L)^2$ and $C_2 = (k_2 L)^2$ two variables to stabilize the division with weak denominator

L - Dynamic range and and $k_2 = 0.03$

$k_1 = 0.01$

M,N - Image Dimensions.

μ_f, σ_f - Mean and standard deviation of the foreground region

μ_b, σ_b -Mean and standard deviation of the background region

μ_h, σ_h - Mean and standard deviation of the homogenous region

A perceptually good quality image has a very high PSNR value. Experimental results show that a high PSNR value is obtained for the proposed method for various noise levels. Table 1, 3 & 5 indicate that the proposed *beta-trim* technique generates high PSNR values even at very high noise levels. The PSNR values of both *soft* and *hard* shrinkage techniques are much lesser in comparison to the proposed *beta-trim* technique. The table also depicts the consistency of the proposed technique at high noise levels.

MSE refers to the noise rejection capability of the de-noising method. MSE value should be as low as possible. A low value of MSE leads to an exact replica of the original image. It is inferred from Table 1, 3 & 5 that the MSE values obtained for beta-*trim* shrinkage are lesser when compared to the existing methods. It can be found that the proposed method is highly effective at high noise levels.

The SSIM is an image fidelity measure, capable of differentiating the structural and non-structural distortions in an image. While non-structural distortions such Gamma distortions, luminance, contrast and spatial shift do not affect structure of the system, Structural distortions such as noise, blur and glossy compression tend to

Table 1.

Parametric Results	Noise Variance		10	20	30
MRI-1	PSNR	hard	28.1	22.1	18.5
		soft	28.2	22.2	18.6
		beta-trim	30.2	26.1	24.4
	MSE	hard	100.2	404.9	902.4
		soft	99.9	404.0	901.2
		beta-trim	61.7	159.3	237.6

Table 2.

Parametric Results	Noise Variance		10	20	30
MRI-1	MSSIM	hard	0.76	0.67	0.48
		soft	0.84	0.78	0.62
		beta-trim	0.92	0.90	0.85
	CC	hard	0.995	0.925	0.855
		soft	0.994	0.935	0.874
		beta-trim	0.996	0.963	0.931

Table 3.

Parametric Results	Noise Variance		10	20	30
MRI-2	PSNR	hard	28.18	22.12	18.55
		soft	28.19	22.13	18.56
		beta-trim	29.44	24.98	22.78
	MSE	hard	99.83	402.5	902.84
		soft	99.67	402.2	902.26
		beta-trim	79.01	240.8	428.23

Table 4.

Parametric Results	Noise Variance		10	20	30
MRI-2	MSSIM	hard	0.74	0.65	0.42
		soft	0.81	0.74	0.59
		beta-trim	0.90	0.88	0.81
	CC	hard	0.994	0.914	0.846
		soft	0.994	0.928	0.862
		beta-trim	0.995	0.961	0.920

Table 5.

Parametric Results	Noise Variance		10	20	30
MRI-3	PSNR	hard	28.06	22.16	18.54
		soft	28.07	22.17	18.55
		beta-trim	29.36	25.04	22.70
	MSE	hard	99.62	397.77	904.76
		soft	99.36	397.18	903.81
		beta-trim	74.89	205.96	342.34

Table 6.

Parametric Results	Noise Variance		10	20	30
MRI-3	MSSIM	hard	0.70	0.61	0.48
		soft	0.80	0.70	0.62
		beta-trim	0.87	0.90	0.76
	CC	hard	0.985	0.906	0.823
		soft	0.985	0.914	0.858
		beta-trim	0.989	0.954	0.914

distort the image significantly. Human visual system tends to be highly sensitive to structural distortions, while non-structural distortions can be compensated. Under such condition retention of signal structure becomes an important image quality metrics. Table 2, 4 & 6 indicate that the proposed shrinkage technique is highly resistant to structural distortions at both high and low noise levels. The Mean SSIM (MSSIM) values of the proposed method are higher than he existing techniques.

Correlation coefficient is a statistical measure of how well the De-noised image follows the trends in the original image. A high value of correlation coefficient indicates a stronger level of relationship between the original and de-noised images. It can be inferred from Table 2, 4 & 6 that the proposed is highly effective in maintaining high correlation coefficient. When compared to *hard* and *soft* shrinkage techniques, the proposed method maintains a high level of correlation coefficient.

MSE refers to the noise rejection capability of the de-noising method. The MSE value should be as low as possible. Table.1, 3 & 5 gives a detailed view of the PSNR and MSE values for different noise levels for the three different MR Images. It is inferred from the table (1, 2 & 3) the MSE values obtained for *beta-trim* shrinkage are

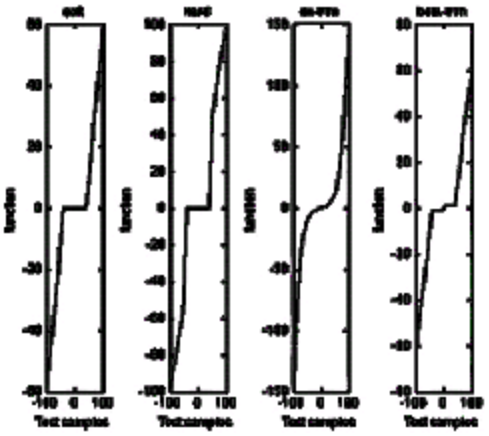

Fig.1. The characteristic shrinkage curve for different shrinkage techniques

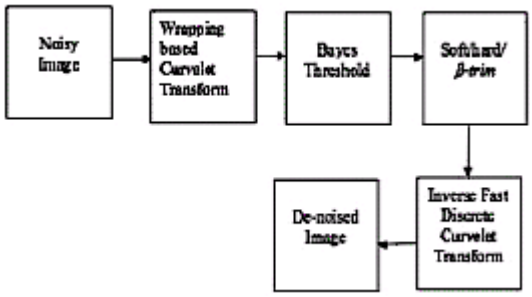

Fig. 2. Block Diagram of Basic De-noising method using Curvelet Transform

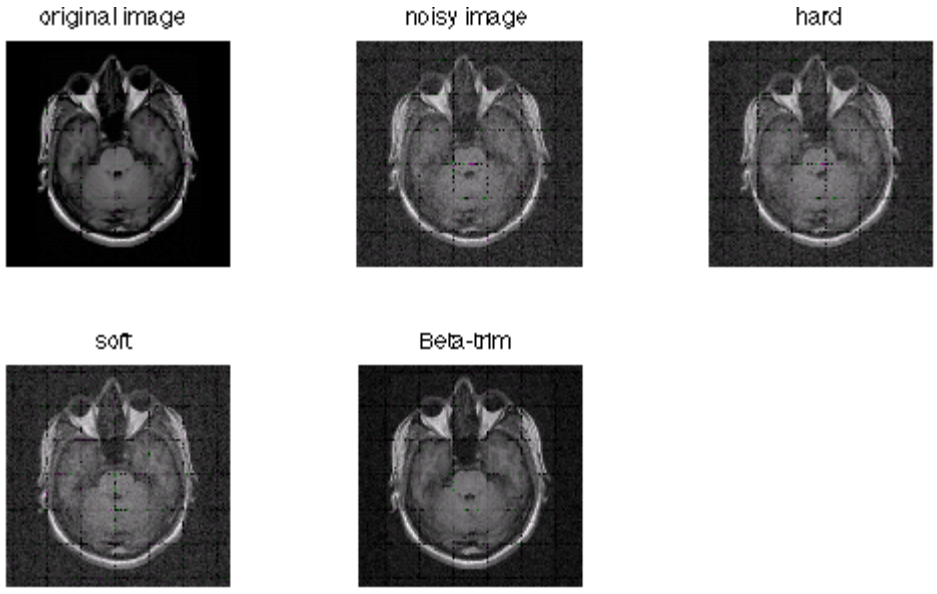

Fig.3. Comparing the performance of *soft, hard* and *beta-trim* with ó=20.

lesser to those of the *soft* and *hard* shrinkage techniques. It can be found from the tables that even at high noise levels the MSE values of the proposed shrinkage technique are maintained at low values. This indicates the stability of the proposed *beta-trim* shrinkage technique.

RESULTS AND DISCUSSION

The experiments were conducted on several images, some of them are discussed here. We consider three 512 x 512 Magnetic resonance images corrupted by Rician noise. The simulation

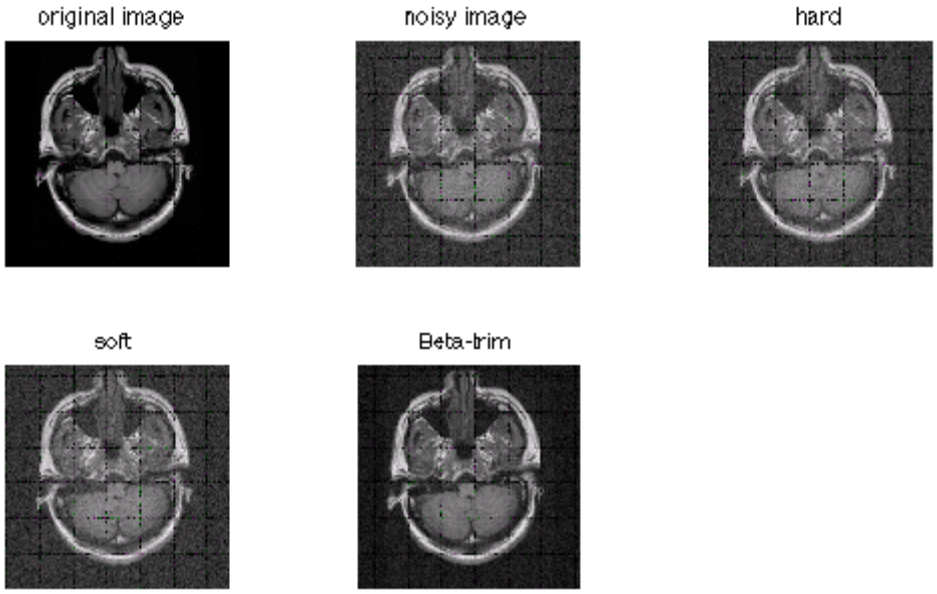

Fig.4. Comparing the performance of *soft*, *hard* and *beta-trim* with ó=20.

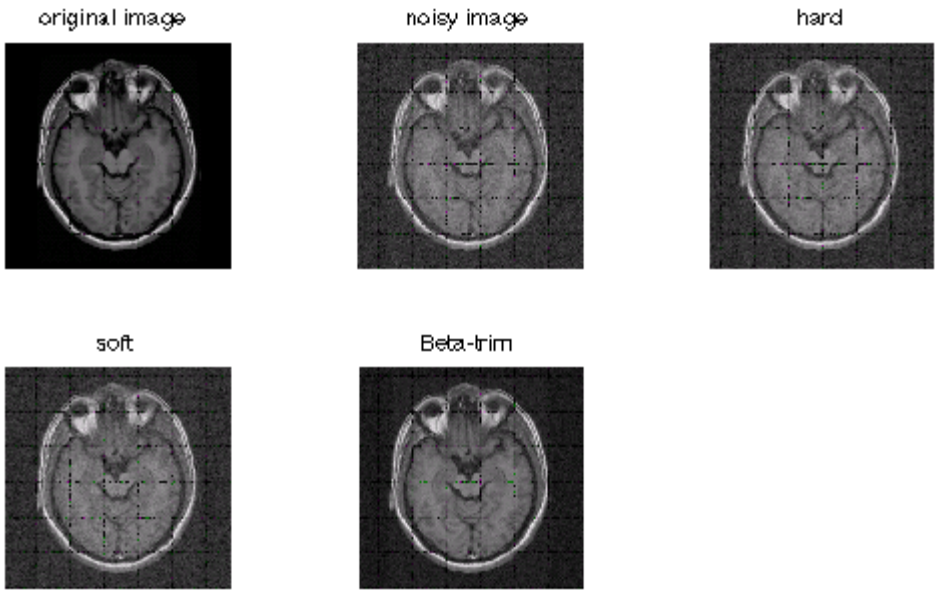

Fig. 5. Comparing the performance of *soft*, *hard* and *beta-trim* with ó=20.

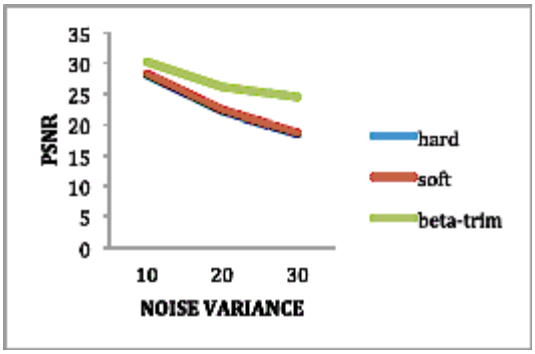

Fig.6. Brain Image (a).PSNR versus Noise Variance

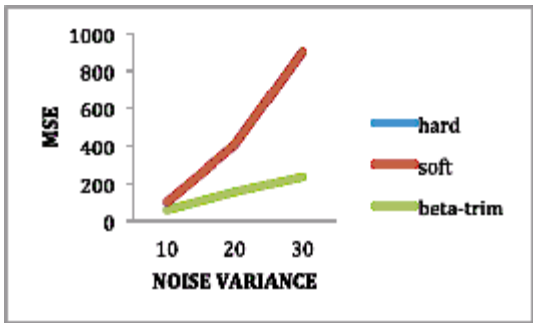

Fig.7. MSE versus Noise Variance

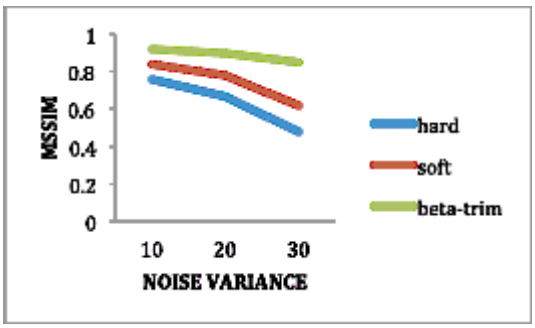

Fig. 8. MSSIM versus Noise Variance

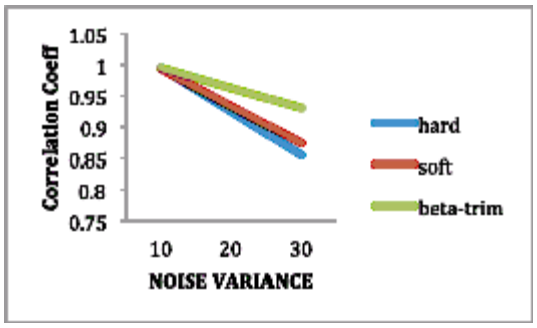

Fig.9. Brain Image (a).Correlation Coefficient versus Noise Variance

was conducted for the different noise levels ranging from 10% to 30% using different shrinkage techniques. In Fig.3, 4 and 5 we compare the de-noised images obtained by applying different shrinkage techniques with a noise level of $\sigma = 20$. The quality of the de-noised image was found to be better, PSNR, MSSIM & Correlation Coefficient values higher, MSE values appreciably lower, were obtained on applying *beta-trim* when compared to its counterparts *hard* and *soft* shrinkage techniques.

Sharper and visually high quality images are obtained on applying *beta-trim* shrinkage. We can infer from figure (3, 4 & 5) that noise speckles in case of *beta-trim* are much lesser when compared to other shrinkage techniques. It can also be found that edges are captured very clearly and there is no smoothening or blurring effect. To illustrate the performance of the proposed method, PSNR, MSE, MSSIM & Correlation coefficient were plotted versus different noise levels for all three shrinkage functions (figures 6-9). A sample MR Image MR-1 is used for this evaluation. It is evident from the figures that the PSNR, MSSIM & Correlation Coefficient values obtained using *beta-trim shrinkage* are much higher than *soft* and *hard* shrinkage and the difference keeps increasing as the noise levels increase. Thus *beta-trim* shrinkage performs consistently even for high noise variance values. In case of figure 6 & 7 the plots for PSNR and MSE values of *soft* and *hard* shrinkage techniques coincide with each other since the difference between the corresponding values is very less.

CONCLUSION

Curvelet transform based image de-noising using *beta-trim shrinkage* was proposed and compared with *hard* and *soft* shrinkage techniques. In all the cases the adaptive Bayesian threshold was used. The proposed method significantly reduces noise while preserving the features in the original image. Experimental results show that the PSNR values obtained for *beta-trim* shrinkage are much higher, more robust and consistent. In addition, the image perception in case of *beta-trim* shrinkage is sharper and better than *soft* and *hard* shrinkage techniques.

The Low MSE values obtained in *beta-trim shrinkage* show that the proposed *beta-trim shrinkage* technique has a high noise rejection capability and is capable of recovering the original image even at high noise levels. The proposed technique proves to be distortion resistant with high SSIM values. The higher values of correlation coefficient indicate higher signal retention capabilities. Thus the proposed *s-trim* method proves to be a simple, efficient method in eliminating noise from Magnetic Resonance Images. The comparison on different quality metrics shows its functional capability of improved performance when compared to the existing methods. A lot of research is being carried out in restoring Optical Coherence Tomography (OCT) images corrupted by speckle noise. The Proposed method can be implemented to enhance such medical diagnosis. The De-noising process can also be enhanced using Graphics Process Unit (GPU) thereby accelerating the algorithm and making it applicable for clinical purposes.

REFERENCES

1. A. Sumaiya and S.Poornachandra, "Image De-Noising Using Ex-Trim Shrinkage", *International Journal of Computing & Information Technology, IJCIT*, 2010; **2**(1).
2. A. Sumaiya and S.Poornachandra, "Optimizing of Image De-Noising Using Ex-Trim Shrinkage", *International Journal of Electronics, Electrical and Communication Engineering, IJEECE*, 2009; ISSN 0975-4814, **1**(1); 43 -50.
3. A.G. Bruce, H. -Y. Gao, WaveShrink with firm shrinkage, *Statist. Sin*, 1997; **7**, pp. 855–874.
4. A.Hyvarinen, J. Karhunen, and E. Oja, "Independent Component Analysis", John Wiley, 2001.
5. Achim, P. Tsakalides and A. Bererianos, "SAR image denoising via. Bayesian wavelet shrinkage based on heavy-tailed modelling, *IEEE Trans Geosci, Remote Sens*, 2003; pp. 1773-1784.
6. B. T. Kelley, V. K. Madisetti, "The Fast discrete Radon transform – I: Theory", *IEEE Trans. On Image Proc.*, 1993; **2**; 382-400.
7. D. Donoho, "Wedgelets: nearly minimax estimation of edges, *Ann. Statistics*, 1999; **27**(3); 859-897.
8. D. L. Donoho and M. R. Duncan, "Digital curvelet transform: strategy, implementation and experiments," in Proc. Aerosense 2000, *Wavelet Applications VII. SPIE,* 2000, **4056**, pp. 12-29
9. D. L. Donoho, I.M.Johnstone, "Ideal spatial adaptation by wavelet shrinkage", *Biometrica*, 1995; **41**(3), pp.613-627.
10. D. Labate, W-Q. Lim, G. Kutyniok, and G. Weiss, "Sparse multidimensional representation using shearlets", SPIE Proc. *Wavelets XI*, 2005; **5914**, pp. 254-262, San Diego, CA
11. D.L. Donoho, De-noising by soft thresholding, *IEEE Trans. Inform. Theory*, 1994; **41**(3); 613–627.
12. D.L.Donoho and I. M. Johnstone, "Adapting to Unknown Smoothness via Wavelet Shrinkage [J]. *Journal of American StatAssoc*, 1995; **12**, pp.1200-1224
13. E. Candes, D. Donoho *et al*, "Curvelets–surprisingly effective non adaptive representation for objects with edges- curves and surfaces", 1999.
14. E. Candes, L. Dermanet, D. Donoho, and L. Ying, "Fast discrete Curvelet transforms," *SIAM Multistage Model. Simul*, 2006; **5**(3); 861-899.
15. E. Le Pennec, S. Mallat, "Sparse geometrical image approximation with bandlets", *IEEE. Trans.Image Process.*, **14**(4); 423-438.
16. E. Simoncelli, W. Freeman, E. Adelson, D. Heeger, "Shiftable multiscale transforms", *IEEE Trans. Inform. Theory*, 1992; **38**(2); 587-607.
17. E.J.Candes and D. L. Donoho. "Ridgelets: the key to higher-dimensional intermittency?" *Phil. Trans. R. Soc. Lond. A.* 1999; **357;** 2495-2509
18. G. Beylkin, "Discrete Radon transform", *IEEE Trans. Acoust. Speech Sig. Proc.*, 1987; **35**; 162-172.
19. J. L. C. Sanz, E. B. Hinkle, and A. K. Jain, Radon and Projection transform-based computer vision, Springer Verlag, 1988.
20. J. Neumann, G. Steidl, Dual-tree complex wavelet transform in the frequency domain and an application to signal classification, Int. J. Wavelets, *Multiresolution and Inform. Process.*, 2005; **3**(1); 43-66.
21. J.L. Starck, E. Candes, and D.L.Donoho, "The Curvelet Transform for image Denoising", *IEEE Trans. Image Processing*, 2002;**11**(6), pp.670-684.
22. Javier Portilla, Vasily Strela, Martin J.Wainwright and Eoro P. Simoncelli. (2002), "Adaptive Wiener De-noising using a Gaussian Scale Mixture Model in the wavelet Domain", Proceedings of the 8th International Conference of Image Processing, Thessaloniki, Greece.
23. K. Guo, D. Labate, "optimally sparse multidimensional representation using shearlets", *SIAM J. Math. Anal.*, 2007; **39**, pp. 298-318.
24. M. N. Do and M. Vetterli, "The contourlet

transform: an efficient directional multiresolution image representation", *Image Processing, IEEE Transactions on,* 2005; **14**: 2091-2106.

25. N. Kingsbury, Complex wavelets for shift invariant analysis and filtering of signals, *Appl. Comput. Harmon. Anal.,* 2001; **10**(3); 234-253 .
26. N. Kingsbury, Image processing with complex wavelets, *Phil. Trans. R. Soc. Lond. A,* 1999; **357**; 2543-2560.
27. R. Willet, K. Nowak, "Platelets: A multiscale approach for recovering edges and surfaces in photon-limited medical imaging", *IEEE Trans. Med. Imaging,* 2003; **22**(3): 332-350.
28. S. G. Chang, B. Yu, and Martin Vetterli, "bridging compression to wavelet thresholding as a denoising method", in proc. Conf. information sciences systems, Baltimore, MD, 1997: 568-573.
29. S. G. Chang, B. Yu, and Martin Vetterli, "Spatially adaptive wavelet thresholding with context modeling for image denoising method", *IEEE Trans. Image Proc,* 2000; **9**; 1522-1531.
30. S. Mallat, G.Peyre, "A review of bandlet methods for geometrical image representation, *Numer. Algorithms,* 2007; **44**(3); 205-234.
31. S.G.Chang, B. Yu and V. Martin, "Adaptive wavelet thresholding for image denoising & compression" *IEEE Trans. Image Proc,* 2000; **9**: 1532-1546.
32. T. Lee, Image representation using 2D Gabor wavelets, *IEEE Trans. Pattern Analysis and Machine Intelligence,* 2008; **18**(10); 1-13.
33. Vladan Velisavljevic, et al. "Directionlets: Anisotropic Multidirectional Representation with Sepearable Filtering", *Image Processing, IEEE Transactions on,* 2006; **15**(7).
34. W. Freeman, E. Adelson, "The design and use of steerable filters, *IEEE Trans. Pattern analysis and Machine Intelligence,* 1991; **13**(9); 891-906.
35. X. Gao, T. Nguyen, G. Strang, "A Study of two channel complex-valued filter banks and wavelets with orthogonolity and symmetry properties, *IEEE Trans Signal Process.,* 2002; **50**(4); 824-833.
36. Y. Chen and C. Han, " Adaptive wavelet thresholding for image denoising", *Electron Lett,* 2007; **41**; 586-587.
37. Y. Lu, M. N. Do, "Multidimensional directional filter banks and surfacelets", *IEEE Trans. Image Process.,* 2007; **16**(4); 918-931.